Comprehensive survey of Nd3+ substitution In La2Mo2O9 oxide-ion conductor

Gwenaël Corbel, Pierrick Durand, Philippe Lacorre

Comprehensive survey of Nd^{3+} substitution in $La_2Mo_2O_9$ oxide-ion conductor

Gwenaël Corbel *, Pierrick Durand, Philippe Lacorre

Laboratoire des Oxydes et Fluorures, UMR-6010 CNRS, Université du Maine, Avenue Olivier Messiaen, 72085 Le Mans Cedex 9, France.

Abstract

Differential thermal analysis coupled to temperature-controlled diffraction have given evidence of a topological metastability phenomenon in an extended compositional range of the $La_{2-x}Nd_xMo_2O_9$ solid solution. A metastable–stable phase diagram is proposed for this series of LAMOX-type fast oxide-ion conductors. In the Nd range $0<x\leqslant 0.35$, a freezing of the oxygen/vacancy disorder of the β-phase at ambient temperature can be achieved through a splat-quenching to water–ice mixture or/and shaping/sintering into pellet. In the intermediate $0.4\leqslant x\leqslant 1.2$ range, the amount of β-metastable phase grows upon substitution for powders. The negative impact of β-metastable to α phase transition on conductivity tends to disappear through the partial stabilization of the β phase by shaping/sintering.

Keywords

$La_2Mo_2O_9$, LAMOX, phase diagram, metastability, internal strain gradient.

Introduction

Nine years ago, Goutenoire and Lacorre had evidenced in $La_2Mo_2O_9$ fast oxide-ion conduction larger at high temperature than that of YSZ8%, the most commonly used electrolyte in fuel cell [1,2]. However, this binary oxide exhibits a reversible $\alpha\rightarrow\beta$ (monoclinic→cubic≡order→disorder) structural phase transition around 580 °C with a ~0.5% abrupt cell volume expansion, detrimental to any electrochemical applications. As a consequence, earlier works were devoted to stabilize at room temperature the highly conducting β-form through cationic site substitution on La or/and Mo sites (LAMOX family) [3].

Partial substitution of La^{3+} by Nd^{3+} has been investigated originally by our group [4] and later by Tsai et al. [5] and Marrero-López et al. [6]. However, these studies led to seemingly contradictory results in terms of phase stability (α for raw powders whatever Nd content and β for pellets with Nd content higher than 30 mol%). Our recent work revealed that the equilibrium of point defects in Ca or Eu substituted LAMOX can be changed by the thermal history or the internal strain induced by the sample shaping [7–9]. A reinvestigation of the $La_{2-x}Nd_xMo_2O_9$ series was undertaken along these lines in order to control the thermal stability, prerequisite to any use as fuel cell core material. At first, temperature-controlled X-ray diffraction allowed to identify the nature of the phases involved in phase transformations detected by differential thermal analysis on raw powder samples. Then, fluctuations in temperature dependencies of the electrical conductivity measured on dense pellet samples by impedance spectroscopy were elucidated thanks to X-ray diffraction performed on these ceramics. Finally, a comprehensive survey of Nd^{3+} substitution in $La_2Mo_2O_9$ oxide-ion conductor was obtained and is reported in the present paper.

Experimental details

Polycrystalline samples of $La_{2-x}Nd_xMo_2O_9$ (two and one compositions per decimal fraction of x, in the 0.05–1 and 1–1.5 ranges, respectively) were prepared by conventional solid state reaction. Prior to use, La_2O_3 and Nd_2O_3 were calcinated in air for 12 h at 1000 °C in order to remove adsorbed water and carbon dioxide. The stoichiometric mixture of La_2O_3, Nd_2O_3 and MoO_3 was first heated, in an alumina crucible, at 500 °C and then at 850 °C for 12 h each. Three additional annealings at 900 °C for 12 h (heating and cooling rates 5 °C/min) with regrindings into acetone in between were necessary to obtain a pure single phase.

After completion, X-ray powder diffraction patterns were recorded at room temperature on a PANalytical θ/θ Bragg-Brentano X'pert MPD PRO diffractometer ($CuK\alpha_{1+2}$ radiations) equipped with the X'celerator detector. Temperature-controlled diffractograms were collected on the same diffractometer equipped with a HTK 1200 Anton Paar chamber from 25 to 1060 °C (under air flow, heating rate of 10 °C/min, temperature stabilisation for 20 min with temperature correction after calibration [10]). Data collection was carried out in the [9°–19°] and [15°–105°] scattering angle ranges with a 0.0167° step over 20 and 108 min, respectively. The program GSAS/EXPGUI [11] was used for pseudo-Rietveld refinements. Note that, the crystal structure of the low temperature form α-$La_2Mo_2O_9$ [12] contains 96 cations and 216 oxygen atoms, while O2 and O3 positions are partially occupied with large anisotropic thermal factors in the structure of

* Corresponding author. Fax: +33 2 43 83 35 06.
E-mail address: gwenael.corbel@univ-lemans.fr (G. Corbel).

the high temperature form β-$La_2Mo_2O_9$ [4]. Because of the complexity of the structures and since X-ray diffraction is less sensitive to oxygen than neutron diffraction, all atomic positions, Mo and oxygen site occupation factors and all thermal factors of the structures of α-$La_2Mo_2O_9$ and β-$La_2Mo_2O_9$ were simply used as structural models. The site occupation factors relative to La crystallographic sites have been changed as a function of the Nd nominal content. Only the cell dimensions, parameters of the pseudo-Voigt profile shape function and the zero shift were refined. The quality of fit was equal all along the series with conventional *R*-factors: $R_{wp} = 4$–6%, $R(F^2) = 8$–11% and $\chi^2 = 1$–3. Additional temperature-controlled diffractograms of the (231) pseudo-cubic peak for raw powder and dense ceramic (13 mm in diameter and 0.8 mm in thickness) of the $x = 0.1$ and 0.3 samples were collected upon heating every 10 °C from RT to 1060 °C in the [46.4°–48.2°] scattering angle range over 371 s with a 0.0084° step (under air flow, heating rate 10 °C/min, temperature stabilisation for 1 min).

Thermal analyses were performed on raw powders with a TGA/DTA Q600 SDT TA Instruments apparatus (Pt crucibles, Al_2O_3 as a reference) under air flow (100 mL/min). Thermograms were collected on ~100 mg samples in the RT–700 °C range (heating/cooling rate of 10 °C/min).

Dense ceramic samples (relative density >95% of theoretical density) were obtained along the method extensively described in reference [9]. After sintering for 3 h at 1050 °C and cooled at 5 °C/min, the phase purity was checked on the pellet by X-ray diffraction.

Thin Pt films electrodes were deposited by RF sputtering on both flat faces of the sintered pellets. Two probe electrical conductivity measurements were carried out using a Solartron 1260 frequency response analyser connected to a Solartron 1296 dielectric interface over the 10 MHz–0.05 Hz range (ac voltage of 50 mV, 40 points/decade). Complex impedance spectra were recorded under dry air flow every 25 °C (35 min thermal equilibration) over the temperature ranges 300–350 and 600–725 °C and every 10 °C in the intermediate range 350–600 °C. Impedance diagrams plotted in the Nyquist complex plane were least squares fitted with a series combination of R//C and R//CPE elements of the Z-view 2.8d software assigned, respectively, to the bulk and grain boundaries contributions [13].

Results and discussion

Powder samples

When raw powder samples were cooled from 900 °C at 5 °C/min, room temperature X-ray diffraction patterns show that the stabilization of the cubic β-form takes place at Nd content

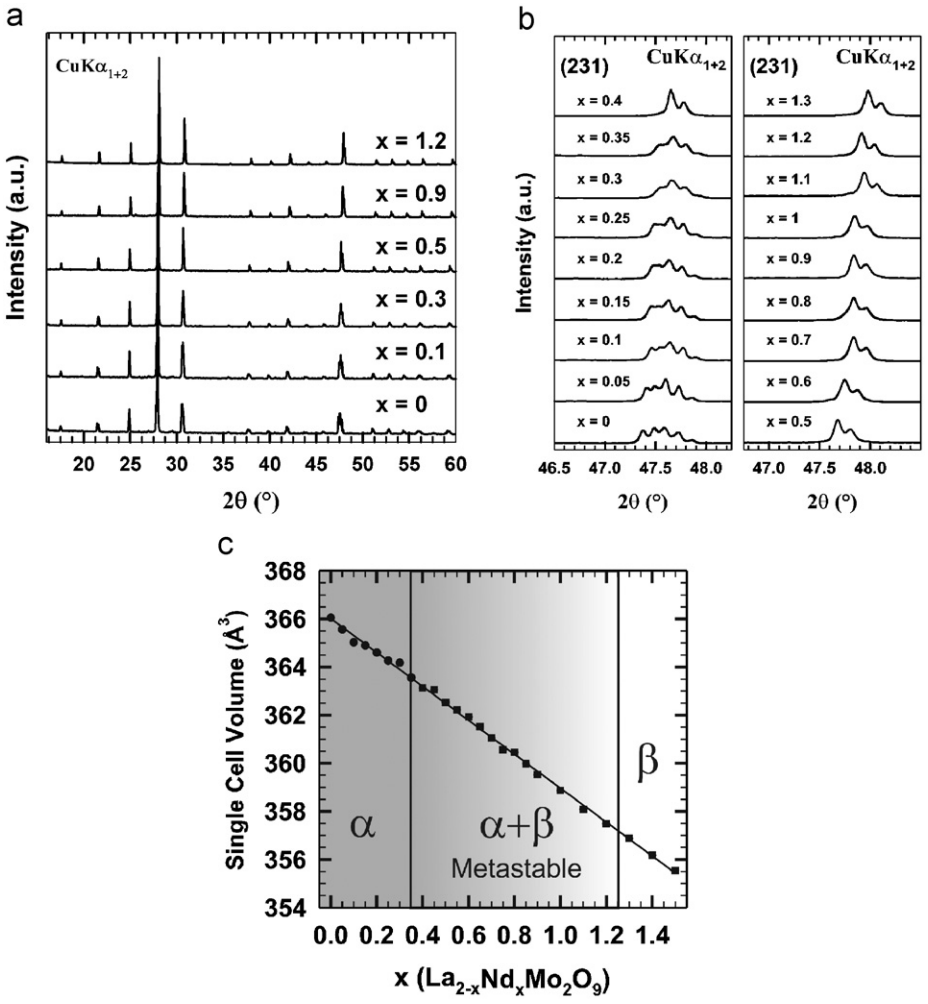

Fig. 1. (a) Room-temperature X-ray diffraction patterns of $La_{2-x}Nd_xMo_2O_9$ for different Nd contents and (b) enlargement of the 2θ region where monoclinic distortion of the α-form is visible. (c) Variations of the single unit cell volume with *x*. Points and squares are obtained from pseudo-Rietveld refinements in a $2 \times 3 \times 4$ monoclinic cell and in a cubic cell, respectively. Errors bars are approximately the size of the data points.

higher than $x = 0.35$. This is clearly demonstrated by the evolution with the substitution rate x of the (231) diffraction line, sensitive to the slight monoclinic distortion of the high temperature β-form (Figs. 1a and b). This observation differs from Georges et al.'s results [4] since in the whole compositional range explored ($0 < x \leqslant 1$), the stabilization of the cubic β-form was never observed at room temperature (see conclusion section). Above $x = 1.5$, weak additional diffraction lines appear at scattering angles around 27.5° and 32.6° which cannot be attributed to any phases reported in JCPDS database. The substitution limit is then considered as exceeded. Pseudo-Rietveld refinements were then carried out either in $2 \times 3 \times 4$ monoclinic supercell (space group $P2_1$; no. 4) [12] for $x \leqslant 0.35$ or in cubic cell (space group $P2_13$; no. 198) [4] for $x \geqslant 0.4$. The linear reduction (Vegard's law, Fig. 1c) of the single unit cell volume with increasing the neodymium content x reflects that Nd^{3+} (ionic radius = 1.163 Å; CN = 9) is slightly smaller than La^{3+} cations (ionic radius = 1.216 Å; CN = 9) [14]. This work confirms that the partial solid solution can be extended to an Nd concentration of $x = 1.5$, as earlier highlighted by Marrero-López et al. [6].

Then, temperature-controlled X-ray powder diffraction was performed to probe the thermal stability of the high temperature β-form for three compositions in the range $0.4 \leqslant x \leqslant 1.5$: $La_{1.5}Nd_{0.5}Mo_2O_9$, $La_{1.1}Nd_{0.9}Mo_2O_9$ and $La_{0.8}Nd_{1.2}Mo_2O_9$. The thermal behaviour of α-$La_{1.7}Nd_{0.3}Mo_2O_9$ powder sample was also investigated since this composition is probably located at the border region between single monoclinic and cubic phases. Fig. 2 displays the thermal evolution, upon heating, of the (231) pseudo-cubic peak of the selected samples and Fig. 3 shows the temperature dependencies of cell volume deduced from pseudo-Rietveld refinements.

Upon heating, a single α/β structural phase transition, characteristic of the parent compound $La_2Mo_2O_9$, is observed for the $x = 0.3$ sample at around 550 °C (Fig. 2a). In the $x = 0.5$ and $x = 0.9$ samples, the broadening of (231) cubic peak, in the intermediate temperature range 450–565 °C and 485–550 °C, respectively, is ascribed to the splitting caused by the monoclinic distortion of the α-phase (Figs. 2b and c). The thermal extent of the stability domain of the α-phase decreases from 115 to 65 °C as the Nd content increases. Within this thermal domain, pseudo-Rietveld refinements were then carried out in a $2 \times 3 \times 4$ monoclinic supercell (open circles in Fig. 3) as for the $x = 0.3$ sample below 550 °C. The reduced cell volume relative to the transient α-phase is found to be slightly smaller than that of the β-phase before the inverse β/α transition. These results point out the metastable character of the β-phase obtained by cooling of

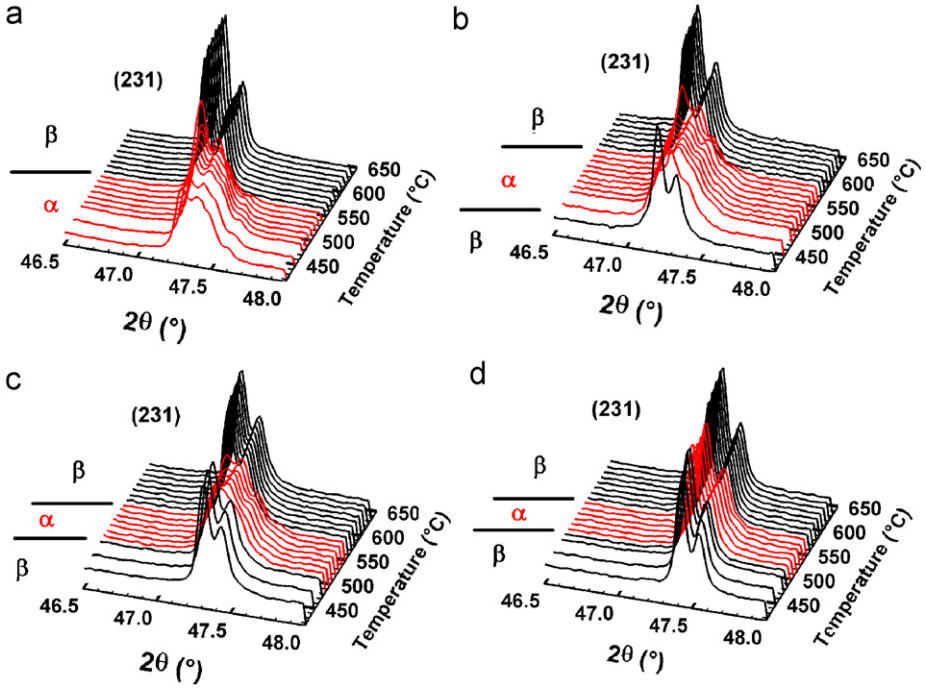

Fig. 2. Thermal evolution, upon heating, of the (231) pseudo-cubic peak for powder samples $La_{2-x}Nd_xMo_2O_9$ (initially cooled at 5 °C/min): (a) $x = 0.3$, (b) $x = 0.5$, (c) $x = 0.9$ and (d) $x = 1.2$.

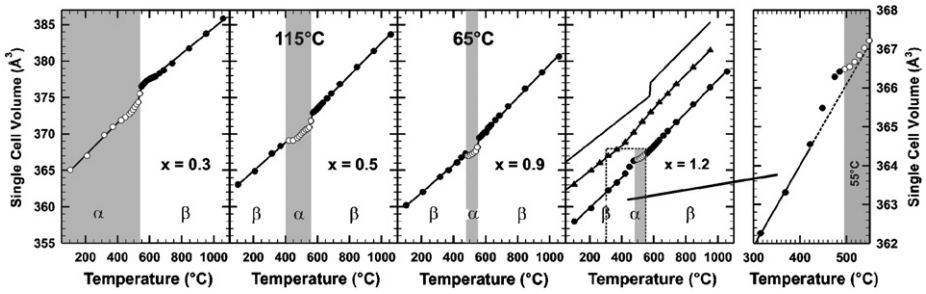

Fig. 3. Temperature dependencies of the single cell volume of $La_{2-x}Nd_xMo_2O_9$ raw powder samples determined from temperature-controlled X-ray diffraction data. For reference, the thermal expansion curves of $La_2Mo_2O_9$ and β-$La_{1.6}Eu_{0.4}Mo_2O_9$ are added as a solid line and triangles, respectively.

powder samples from 900 °C at 5 °C/min. This topological metastability was already highlighted for trivalent Eu substituted $La_2Mo_2O_9$ in a narrower compositional range of 2.5 mol% (Fig. 5c) [9].

In comparison, diffuse double $\beta/\alpha/\beta$ transitions upon heating were detected for the $x = 1.2$ sample (Fig. 2d). Only a slight reduction in intensity of the (231) cubic peak occurs in the temperature range 495–550 °C with a small widening of its base. However, pseudo-Rietveld refinements were performed in a cubic cell whatever the temperature considered. In Fig. 3, it is worth noting that the thermal evolution of cell volume for the $x = 1.2$ sample displays a diffuse bump in the temperature range 425–555 °C. This behaviour differs from stable cubic members of the LAMOX family. For instance in the β-$La_{1.6}Eu_{0.4}Mo_2O_9$ sample [9] (triangles in Fig. 3), at temperatures higher than 420 °C, an extra volume expansion relative to the linear cell volume expansion at low temperatures (RT-420 °C) is associated to a pronounced departure from Arrhenius behaviour in conductivity curve. This change could possibly originate from a transition from static to dynamic disordering of oxygen vacancies involved by the cationic framework distortion/libration without symmetry breaking (Arrhenius to Vogel–Tammann–Fulcher (VTF) mechanisms [9,15,16]).

For $La_{0.8}Nd_{1.2}Mo_2O_9$, the bump in the thermal expansion is interpreted as a frustration of the Arrhenius/VTF transition. It is likely that the cell volume decrease above 480 °C is representative of the conversion of the low temperature β-phase into a weakly monoclinic distorted α-phase. Thereby, once again for $x = 1.2$, the metastability of the low temperature β-phase is retained.

In the light of the results reported for samples within the Nd range $0 \leqslant x \leqslant 0.35$, a cooling rate of 5 °C/min is not rapid enough to configurationally freeze the disorder existing at temperatures higher than 580 °C. An attempt to quench the high temperature β-phase of $La_{1.9}Nd_{0.1}Mo_2O_9$ powder was undertaken. The powder heated at 900 °C was splat-quenched to water–ice mixture. After completion, temperature-controlled X-ray diffraction patterns of the (231) pseudo-cubic peak were collected upon heating. Fig. 4b shows that, when powder is splat-quenched, a single β-type phase is obtained at room temperature which undergoes a complete conversion to monoclinic α-form in a twice larger thermal range $\approx$345–575 °C than for $La_{1.5}Nd_{0.5}Mo_2O_9$.

The asymmetry of (231) diffraction line detected by Marrero-López et al. [6] for $x = 0.5$ or 1 powder samples is more pronounced than we observed (Fig. 1). These authors considered that this asymmetry was a trace of the slight monoclinic distortion and then carried out Rietveld refinements in a monoclinic single cell. However, in our study of $La_{1.85}Eu_{0.15}Mo_2O_9$ samples (cooled at 5 °C/min) [9] by electron microscopy, we have shown that this asymmetry originates from the coexistence of the two polymorphs α and β at ambient temperature. This situation could hence occur within the $La_{2-x}Nd_xMo_2O_9$ series above $x = 0.4$ in particular when powder samples are slowly cooled at 1–2 °C/min as performed by Marrero-López et al. [6] (decreasing the cooling rate favours the growth of the thermodynamically stable α-phase). In our series, no evident overlap of (231) peaks belonging to α and β forms is detected in the diffractograms of Fig. 1, the cooling rate of 5 °C/min acting most probably as a quenching effect. In any case, increasing the substitution rate x from 0.4 to 1.2 would decrease progressively the ratio (low temperature form α/high temperature form β) making more and more difficult the detection of residual monoclinic α-phase.

In order to determine the global behaviour of the whole sample series, systematic recordings of DT thermograms were carried out on large powder samples (~100 mg). In the Nd range $0 \leqslant x \leqslant 0.35$, thermal analyses confirm that the monoclinic α-form is the most thermodynamically stable phase. Upon the increase of cationic disorder with the La^{3+}/Nd^{3+} substitution, a typical broadening and a reduction in intensity of the endothermic peak associated to the first order $\alpha \rightarrow \beta$ transition in $La_2Mo_2O_9$, is observed (Fig. 5a). Above $x = 0.4$, an additional wide peak at lower temperature 400–500 °C appears while the intensity of the peak ascribed to $\alpha \rightarrow \beta$ transition decreases continuously before disappearing above $x = 1.3$ (Fig. 5a).

Thanks to temperature-controlled X-ray diffraction, this first endothermic event can be ascribed to the metastable α/β transition for compositions in the range $0.4 \leqslant x \leqslant 1.2$. In the Nd-richer range ($1.2 < x \leqslant 1.5$), this transition progressively changes into a thermal trace of the postulated Arrhenius/VTF transformation [9,15] of transport mechanism. This explains the disappearance of the peak associated to the α/β transition and was confirmed by the recording of the thermal evolution of the (231) cubic reflection for the $x = 1.3$ sample, which remains unchanged in the whole thermal range RT–1060 °C. Note that the DSC curve reported by D. Marrero-López et al. [6] on β-$La_{0.5}Nd_{1.5}Mo_2O_9$ is in good agreement with the current study. However, these authors ascribed this event at $\approx$500 °C to a reminiscence of the α/β transition (low enthalpy of 0.6 kJ/mol) although that they observed the characteristic change in cell volume expansion of cubic LAMOX above this temperature (expand of the cationic framework associated to Arrhenius/VTF transformation [9,15]).

Then, a complete metasble–stable phase diagrams of the solid solution $La_{2-x}Nd_xMo_2O_9$ is proposed in Fig. 5b. It is noteworthy that the thermal extents of each phase domain are in a good agreement with those determined by diffraction. Fig. 5b shows a monotonous shift towards higher temperature of the metastable β/α transition regardless of the increasing value of x. At reverse,

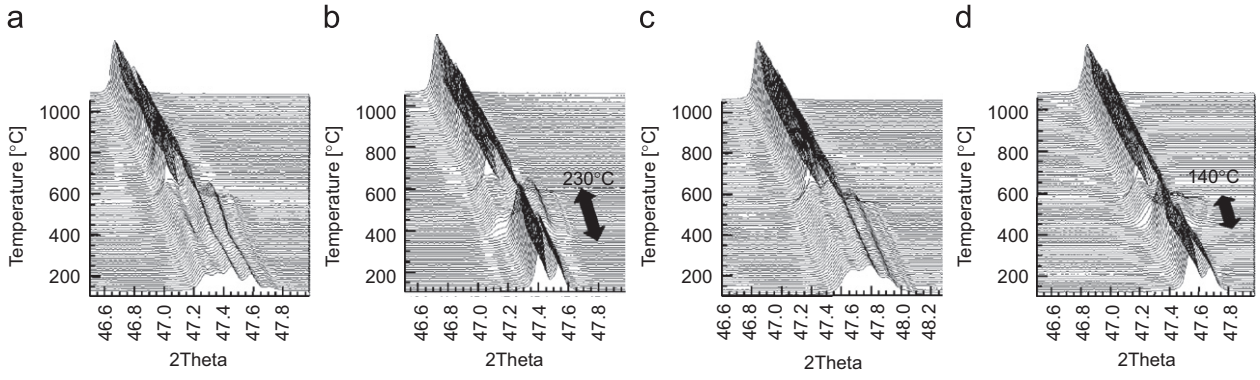

Fig. 4. Thermal evolution, upon heating, of the (231) pseudo-cubic peak of $La_{1.9}Nd_{0.1}Mo_2O_9$ for (a) raw powder sample cooled from 900 °C at 5 °C/min, (b) previous powder sample quenched to water–ice mixture from 900 °C, (c) dense ceramic sintered at 1050 °C and cooled at 5 °C/min and (d) previous dense ceramic quenched to water–ice mixture from 900 °C.

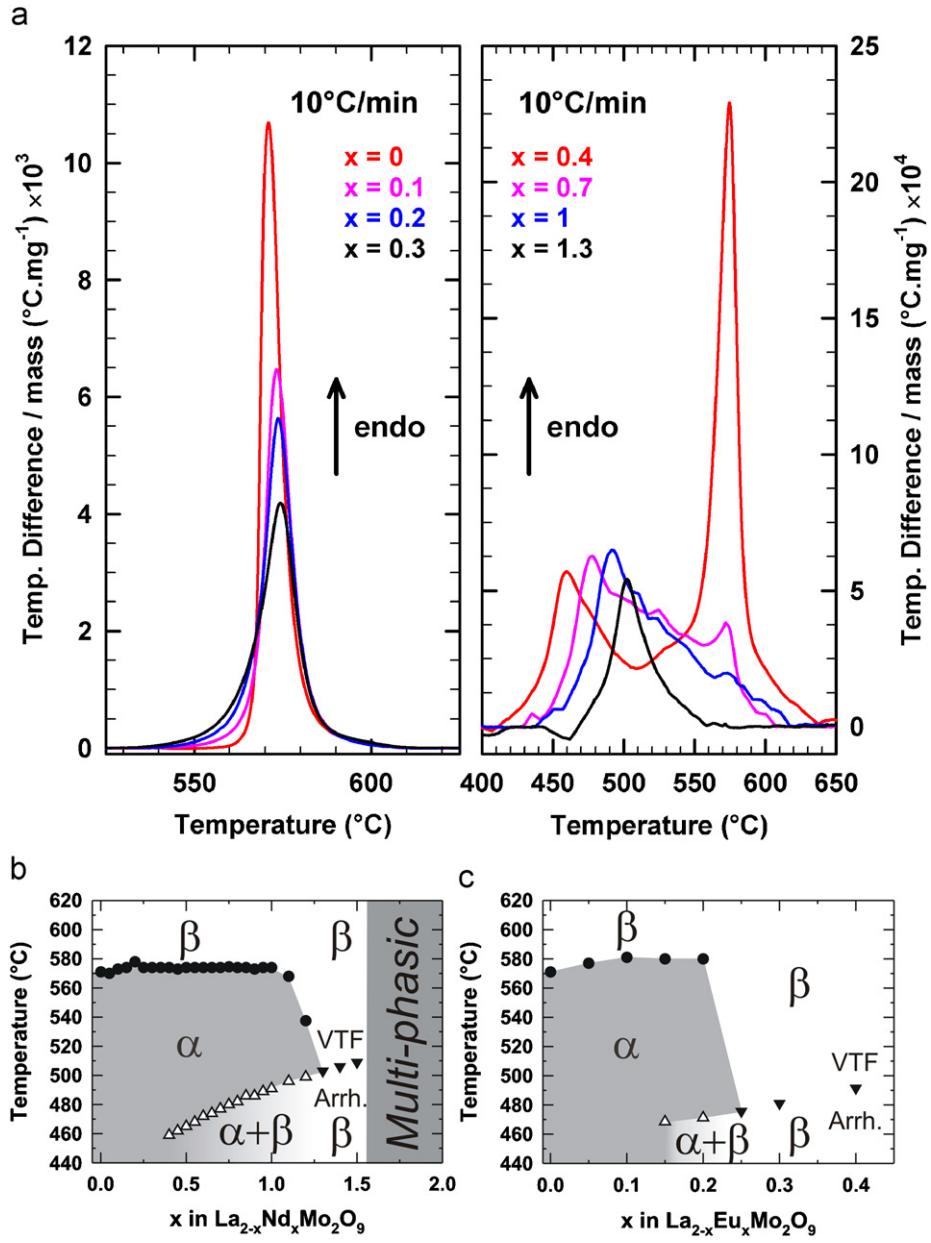

Fig. 5. On raw powders initially cooled down at 5 °C/min : (a) DTA thermograms upon heating of $La_{2-x}Nd_xMo_2O_9$ samples. Background has been subtracted. (b) Metastable-stable phase diagram of the solid solution $La_{2-x}Nd_xMo_2O_9$ determined from DTA. (c) For reference, the phase diagram of the $La_{2-x}Eu_xMo_2O_9$ series, built up from DTA data displayed in [9], is added. Reported transition temperatures were determined at the peaks maximum.

the inverse α/β transition remains almost constant up to an Nd content of $x = 1$ before suddenly falling down above this value.

The compositional range (~40 mol% Nd) where the topological metastability occurs in $La_{2-x}Nd_xMo_2O_9$ series is larger than that observed for trivalent europium substituted $La_2Mo_2O_9$ (~2.5 mol% Eu; Fig. 5c). The much smaller difference in size between Nd^{3+} and La^{3+} (0.053 Å) in comparison with Eu^{3+}/La^{3+} substitution (0.096 Å) might be considered as one plausible explanation of the retaining, over an extended Nd content range, of the metastable character of the β-phase.

Ceramic samples

As shown earlier for $La_{1.9}Nd_{0.1}Mo_2O_9$, increasing the cooling rate changes the equilibrium of point defects since the stress induced by the splat-quenching allows the existence of a β-metastable phase at room temperature. Our recent work revealed that the equilibrium of point defects in Ca or Eu substituted LAMOX can also be stressed by the internal strain induced by the sample shaping/sintering [7,9]. For instance, whereas raw powders of $La_{1.92}Ca_{0.08}Mo_2O_{8.96}$ or $La_{1.8}Eu_{0.2}Mo_2O_9$, both cooled at 5 °C/min, are metastable, the mechanical constraints involved by the compaction into dense ceramics (relative density > 95%) make the permanent stabilization of the β-type phase possible in the whole thermal range RT–950 °C. In this way, a further investigation of the thermal stability of dense ceramic samples appears as a prerequisite to well explain the temperature dependence of conductivity of the $La_{2-x}Nd_xMo_2O_9$ series. Temperature-controlled X-ray diffractograms were recorded on large dense pellets (13 mm in diameter) of $La_{1.9}Nd_{0.1}Mo_2O_9$ and $La_{1.7}Nd_{0.3}Mo_2O_9$.

In Fig. 4(c), pellet of $La_{1.9}Nd_{0.1}Mo_2O_9$ (cooled down at 5 °C/min) behaves the same way as raw powder: a single α/β structural

phase transition upon heating is observed. At reverse, two successive transitions β/α and α/β were noted at 410 and 565 °C, respectively, for $La_{1.7}Nd_{0.3}Mo_2O_9$ ceramic (Fig. 6(b)). The shaping/sintering has therefore involved a metastability of the β-phase. Furthermore, the (231) cubic peak exhibits a weak asymmetry at low scattering angle in the temperature RT–410 °C (Fig. 6(b)) attributed to the coexistence of α and metastable-β phases. For both powder and ceramic samples of $La_{1.9}Nd_{0.1}Mo_2O_9$, only a splat-quenching is able to retain in a metastable state the high temperature β-phase at room temperature (Fig. 4). It is noteworthy that the thermal extent of α-phase domain is lowered by 90 °C when the sample is compacted into pellet.

The thermal dependencies of the overall electrical conductivity of selected compositions are presented in Fig. 7. At 725 °C, the substitution of a 15 mol% fraction of lanthanum for neodymium involves a large decrease by about one order of magnitude of the ionic conductivity relative to pure $La_2Mo_2O_9$. The increase of the Nd content up to $x = 1.2$ tends to continuously reduce this difference in conductivity without never attaining the value measured for $La_2Mo_2O_9$. A correlation between the lowering of conductivity and the porosity is ruled out since a constant relative density of 96(1)% is measured within this series. This observation is in good agreement with the only conductivity curve reported in literature by Marrero-López et al. for dense $LaNdMo_2O_9$ ceramic (relative density of 98%) [6]. Note that the decrease of conductivity for $La_{1.7}Eu_{0.3}Mo_2O_9$ sample ($r(Eu^{3+}) = 1.12$ Å; CN = 9 [14]) is less pronounced than for the 15 mol% Nd substituted analogue ($r(Nd^{3+}) = 1.163$ Å; CN = 9 [14]). A comparison of both series suggests that the content of substitute with highest conductivity would increase with increasing the substitute ionic radius. In order to confirm this tendency, additional work is needed.

In the conductivity curve of $La_{1.7}Nd_{0.3}Mo_2O_9$ sample, a transient low conducting regime is shown in the thermal range 475–565 °C. This sudden decrease of conductivity is ascribed to the appearance of the low conducting monoclinic α-phase, originating from the metastability of the β-phase detected by temperature-controlled diffraction experiment (Fig. 6(b)). The situation becomes more complex when Nd content increases from $x = 0.5$ to 1.2. Indeed, only a bump at around 475 °C is observed on the thermal evolution of conductivity for $x = 0.5$ and 0.9, which becomes diffuse for $x = 1.2$.

One can assume that this bump is a reminiscence of metastability. A pellet was then heated in the temperature range 500–550 °C for 12h (heating rate 5 °C/min) and slow cooled down to room temperature at 0.5 °C/min in order to preserve the thermodynamically stable α-phase. After completion, the flat surface of the pellet was analysed by X-ray diffraction (pattern collected in the [46°–48.5°] scattering angle range over 1748 s with a 0.0084° step). However, the diffractograms of the characteristic (231) reflexion, sensitive to monoclinic distortion, remains unchanged after post-annealing: no trace of splitting or broadening is observed in Fig. 8. Isostatic pressing and sintering of cylindrical compacts are known to generate radial, axial and hoop stress gradients with maximal stress at the top/bottom and lateral

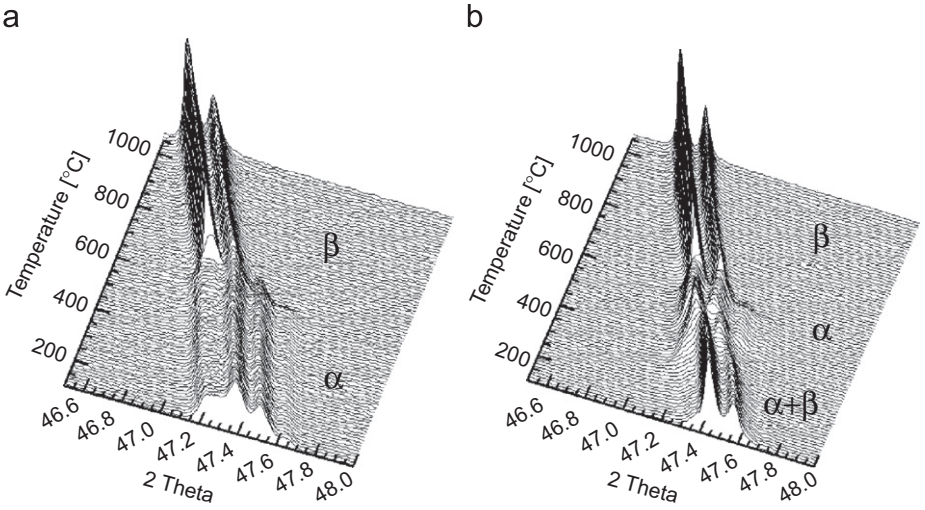

Fig. 6. Thermal evolution, upon heating, of the (231) pseudo-cubic peak of $La_{1.7}Nd_{0.3}Mo_2O_9$ for (a) raw powder sample cooled from 900 °C at 5 °C/min and (b) dense ceramic sintered at 1050 °C and cooled at 5 °C/min.

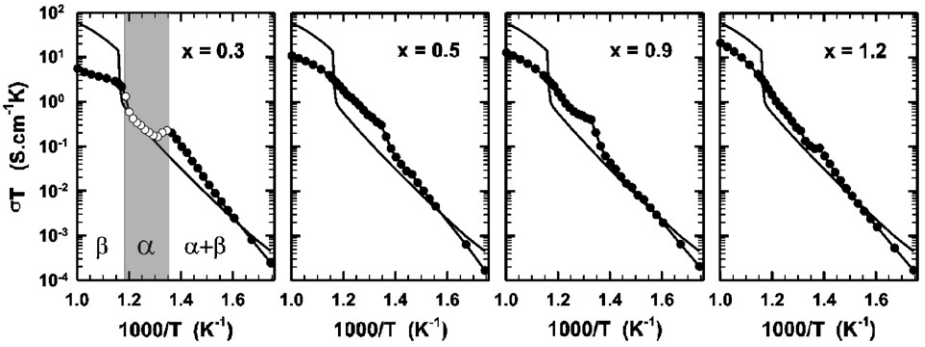

Fig. 7. Temperature dependencies of the electrical conductivity measured in air on dense ceramics of selected members of the $La_{2-x}Nd_xMo_2O_9$ series. The conductivity curve of $La_2Mo_2O_9$ is added as solid line for reference.

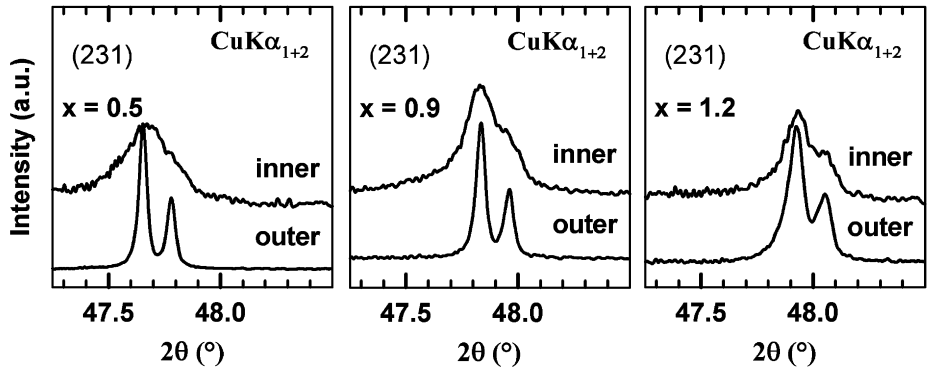

Fig. 8. Room temperature X-ray patterns collected on outer and inner parts of $La_{2-x}Nd_xMo_2O_9$ dense ceramics (see details in the text).

surfaces of the cylinder (peripheral area) and minimal stress at its center (middle area) [17]. Therefore, the recorded XRD diagrams can be considered as mainly representative of the stressed top layer of the pellets. As a matter of fact, the absence of any significant line broadening relative to powder diffraction lines suggests that the stress is uniform within this layer. The difference in stress between the peripheral area and the middle area of the pellets could be responsible for a difference in point defect equilibrium with, for instance, a β-type peripheral area and an α-type middle area (or, depending on cooling rate, a stable β-type peripheral area and a metastable β-type middle area). This could explain some discrepancies observed between the thermal evolution of XRD patterns (peripheral area) and conductivity curves (peripheral+middle areas). In order to check for the existence of such heterogeneity, pellets of $x = 0.5$, 0.9, 1.2 were cut in half parallel to their flat surfaces with a vertical ESCIL W3242 dicing saw equipped with a diamond wire. Then, diffractograms were recorded on the whole internal circular cross section (see Fig. 8). A broadening of (231) pseudo-cubic peak relative to the top surface peak is observed for all specimens. The origin of such a broadening can be threefold. It can come either from a superimposition of α and β peaks due to low-stress central and stressed peripheral areas of the surface or from the effect of stress gradient on the peak width of an homogeneous β-type pellet, or from defects generated by saw cutting. In any case, complementary studies would be necessary in order to determine what hypothesis is correct, or if two or more contribute.

We can, however, attempt to explain the uneven thermal evolution of conductivity using the second hypothesis (homogeneous β pellet). It must be noticed that electrical conductivities were measured on ceramic sintered at 1050 °C and cooled down at 5 °C/min. The proportion of β (metastable or stable) phase is hence larger than after the subsequent annealing at 550 °C and cooling at 0.5 °C/min. Thereby, the singular evolution of the conductivity below $1000/T \approx 1.4\,K^{-1}$ could originate from the central metastable β-phase which becomes stable α, or the stress gradient relief with temperature. The $x = 0.3$ sample stands apart from the $x = 0.5$, 0.9 and 1.2 samples since only the α-form is present within the compact before sintering for the former while α+β-metastable polymorphs coexist for the later. Then, the maximal stress in the peripheral region of compact generated by sintering makes possible either the occurrence of a fraction of β-metastable phase for $La_{1.7}Nd_{0.3}Mo_2O_9$ at the flat surface of the ceramic (Fig. 6(b)) or the stabilization of the β-phase for the $x = 0.5$, 0.9 and 1.2 specimens (detected at room temperature by diffraction, Fig. 8). The higher the proportion of β-metastable phase within pellet before sintering, the larger the amount of β-stable phase within dense ceramic. This is well illustrated by the thermal evolutions of conductivity, typical of a cubic LAMOX member, reported for metastable $La_{1.92}Ca_{0.08}Mo_2O_{8.96}$ [7] and $La_{1.8}Eu_{0.2}Mo_2O_9$ [9] samples.

Conclusions

In this paper, the solid solution $La_{2-x}Nd_xMo_2O_9$ was re-examined with the aim of explaining the seemingly contradictory results in literature. Differential thermal analysis and temperature-controlled X-ray diffraction were systematically used to probe the thermal stability of raw powders cooled at 5 °C/min. This substantial investigation allowed us to draw the first phase diagram for $La_{2-x}Nd_xMo_2O_9$ samples. An evidence of a metastable domain over a ~40 mol% Nd extended compositional range ($0.4 \leqslant x \leqslant 1.2$) was given. In the Nd range $0 < x \leqslant 0.35$, only a splat-quenching to water–ice mixture of raw powders can freeze the oxygen/vacancy disorder of the β-phase at ambient temperature.

To be integrated as core materials in fuel cell or in any electrochemical devices, operating at intermediate temperatures around 500–700 °C, the thermal stability of ceramic membranes or thin films is also of vital importance. In literature, very few studies are devoted to the thermal stability of shaped materials. As pointed out by Lubomirsky [18], application of an external stress could have a non-negligible influence on the defects equilibrium in ionic conductors with high concentration of point defects. Thus, ceramic could expand or contract as the defects equilibrium changes, inducing mechanical stress between device components or in extreme case fracture of the membrane. Our previous work revealed that sample shaping/sintering can turn into stable state an initial metastable Ca or Eu substituted β-LAMOX [7–9]. The Nd–LAMOX series provides the opportunity to gain better insight into this phenomenon. In the Nd range $0 < x \leqslant 0.35$, a freezing of the oxygen/vacancy disorder of the β-phase in a metastable state at ambient temperature can be achieved through shaping/sintering into pellet all the more that x is higher. In the compositional range $0.4 \leqslant x \leqslant 1.2$, the amount of β-metastable phase growing upon substitution for powders, the negative impact of β-metastable to α phase transition on conductivity tends to disappear through the partial stabilization of the β phase by shaping/sintering.

In the study of La^{3+}/Nd^{3+} substitution performed by S. Georges et al. [19], well mixed reactants or calcined powders were systematically uniaxially pressed into pellet to ensure a better reactivity during annealings. The final heating was followed by natural cooling of the furnace. A curious splitting variation of the (231) pseudo-cubic peak was then reported within the range $0.4 \leqslant x \leqslant 1$ and was originally ascribed to a reduction of the monoclinic distortion upon substitution. Since the thermal history

and the sintering effect are able to generate gradients inside pellets, the coexistence of both (α+β) polymorphs can be evoked to explain this singular evolution. Thereby, the endothermic event at 490–500 °C reported by Georges et al. [4] for Nd content higher than 0.8 must be re-attributed to β-metastable/α transition. The non-observation of the α/β transition arises probably from its weakening upon substitution and from the small amount of powder ($\approx$50 mg) used for DTA. In the present study, a comprehensive survey of Nd^{3+} substitution in $La_2Mo_2O_9$ fast oxide-ion conductor was presented reconciling earlier Georges et al. work with Marrero-López et al. study.

Acknowledgment

The authors express their thanks to B. Boulard for her help in pellet cutting operation.

References

[1] P. Lacorre, F. Goutenoire, O. Bohnké, R. Retoux, Y. Laligant, Nature 404 (2000) 856.
[2] F. Goutenoire, O. Isnard, R. Retoux, P. Lacorre, Chemistry of Materials 12 (2000) 2575.
[3] F. Goutenoire, O. Isnard, E. Suard, O. Bohnké, Y. Laligant, R. Retoux, P. Lacorre, Journal of Material Chemistry 11 (2001) 119.
[4] S. Georges, F. Goutenoire, F. Altorfer, D. Sheptyakov, F. Fauth, E. Suard, P. Lacorre, Solid State Ionics 161 (2003) 231.
[5] D.S. Tsai, M.J. Hsieh, J.C. Tseng, H.Y. Lee, Journal of the European Ceramic Society 25 (2005) 481.
[6] D. Marrero-López, J. Canales-Vásquez, W. Zhou, J.T.S. Irvine, P. Núñez, Journal of Solid State Chemistry 179 (2006) 278.
[7] A. Selmi, G. Corbel, P. Lacorre, Solid State Ionics 177 (2006) 3051.
[8] A. Selmi, G. Corbel, S. Kojikian, V. Voronkova, E. Kharitonova, P. Lacorre, European Journal of Inorganic Chemistry 11 (2008) 1813.
[9] G. Corbel, E. Chevereau, S. Kodjikian, P. Lacorre, Inorganic Chemistry 46 (2007) 6395.
[10] G. Corbel, S. Mestiri, P. Lacorre, Solid State Sciences 7 (2005) 1216.
[11] A.C. Larson, R.B. Von Dreele, General structure analysis system (GSAS), Los Alamos National Laboratory Report LAUR 86-748 (1994);
B.H. Toby, Journal of Applied Crystallography 34 (2001) 210.
[12] I.R. Evans, J.A.K. Howard, J.S.O. Evans, Chemistry of Materials 17 (2005) 4074.
[13] Z-View 2.8d, Scribner Associates Inc.
[14] R.D. Shannon, Acta Crystallographica Section A 32 (1976) 751.
[15] S. Georges, F. Goutenoire, O. Bohnké, M.C. Steil, S.J. Skinner, H.D. Weimhöfer, P. Lacorre, Journal of New Materials for Electrochemical Systems 7 (2004) 51.
[16] P. Lacorre, A. Selmi, G. Corbel, B. Boulard, Inorganic Chemistry 45 (2006) 627.
[17] I. Yu. Prokhorov, Journal of European Ceramic Society 19 (15) (1999) 2619;
M. Gasik, B. Zhang, Computational Materials Science 18 (2000) 93.
[18] I. Lubomirsky, Solid State Ionics 177 (2006) 1639.
[19] S. Georges, Ph.D. Thesis, University of Le Mans, France, 2003.